Chemistry–A European Journal
Research Article
doi.org/10.1002/chem.202402868
Chemistry Europe
European Chemical Societies Publishing
www.chemeurj.org

Effect of Oriented External Electric Field in Altering Magnetic Exchange and Magnetic Anisotropy in Lanthanide-Radical Complexes

Tanu Sharma,[a] Ananya Singh,[a] and Gopalan Rajaraman*[a]

Magnetic exchange coupling (*J*) is one of the important spin Hamiltonian parameters that control the magnetic characteristics of single-molecule magnets (SMMs). While numerous chemical methodologies have been proposed to modify ligands and control the *J* value, and magneto-structural correlations have been developed accordingly, altering this parameter through non-chemical means remains a challenging task. This study explores the impact of an Oriented-External Electric Field (OEEF) on over twenty lanthanide-radical complexes using Density Functional Theory (DFT) and *ab initio* Complete Active Space Self-Consistent Field (CASSCF) methods. Five complexes – $[\{(Me_3Si)_2N\}_2Gd(THF)\}_2(\mu\text{-}\eta^2\text{:}\eta^2\text{-}N_2)]$ (**1**), $[Gd(Hbpz_3)_2(dtbsq)]$ (**2**), $[Gd(hfac)_3(IM\text{-}2py)]$ (**3**), $[Gd(hfac)_3(NITBzImH)]$ (**4**), and $[Gd(hfac)_3\{2Py\text{-}NO\}(H_2O)]$ (**5**) – were selected for detailed analysis, revealing significant OEEF effects on magnetic exchange interactions and structural parameters. Various parameters such as bond distances, bond angles, and torsional angles were examined as a function of OEEF to establish guiding principles for molecule selection. In complexes **1**, **2**, and **3**, OEEF influenced torsional angles and altered exchange interactions. Complex **4** demonstrated enhanced ferromagnetic coupling under OEEF, reaching a maximum *J* value of $+5.3\ cm^{-1}$. Complex **5** reveals switching the sign of $J_{Gd\text{-}rad}$ exchange interaction from antiferromagnetic to ferromagnetic under OEEF, highlighting the potential of electric fields in designing materials with tuneable magnetic properties. These findings offer valuable insights for future research and applications in advanced materials and molecular electronics.

Introduction

A key aspect in the realm of single-molecule magnets is the magnetic exchange coupling (*J*),[1] which governs the collective magnetic properties of these complexes.[2] The *J* values are significantly affected by factors such as the type of bridging ligand (e.g., oxo,[3] phenoxo,[4] azide,[5] carboxylates,[6] dicynamato, and cyanide,[7,8] metal-ligand bond lengths, bond angles formed by bridging atoms, dihedral angles between coordination planes, among other parameters.[9] While it is feasible to modify these factors chemically, the process is often challenging. As a result, there is a sustained interest in non-chemical methods to tune these parameters.[10] One such method is employing pressure to alter structural parameters,[11] which in turn alters the exchange coupling parameters. However, challenges such as directing pressure precisely and dealing with intermolecular interactions and crystal quality can impact the outcomes. An alternative approach is using an Oriented-External Electric Field (OEEF) as has been employed by some of us in the past,[12] which can induce structural modifications influencing magnetic exchange interactions, as demonstrated in previous studies.[13]

The experimental manipulation of magnetic exchange in helical 3 d-radical chains using an electric field highlights the potential of this method for quantum computing applications, thus encouraging further exploration of suitable candidates.[13] Quantum computation is positioned at the cutting edge of future information technology, with molecular magnets showing immense potential as advanced qubits that could surpass traditional systems.[14] Despite this promise, the spatial constraints of magnetic fields limit their efficacy in controlling electron spins. Conversely, electric fields provide a practical solution with superior spatial resolution.[13,15] While there is experimental evidence supporting the manipulation of magnetic properties by electric fields[12–13], a comprehensive understanding of how molecules respond to these conditions and how this influences their magnetic properties remains elusive. This understanding is crucial for the progression of electric field-based applications and forms the core focus of this study. Lanthanide SMMs exhibit notable blocking temperatures (T_B),[16] yet they are susceptible to zero-field tunnelling, which can be mitigated by inducing *J*. However, these systems often display primarily antiferromagnetic behaviour with small *J* values.[17] This study analyses five lanthanide-radical complexes subjected to an external electric field using a combination of Density Functional Theory (DFT) and *ab initio* Complete Active Space Self-Consistent Field (CASSCF) methods. We aim to uncover the principles dictating the reversal of magnetic exchange signs, achieve larger *J* values, and propose ways to tune this parameter.

We have studied twenty lanthanide-radical complexes out of 37 molecules reported in the literature (Table S1 in ESI).

[a] *T. Sharma, A. Singh, G. Rajaraman*
Department of Chemistry, Indian Institute of Technology Bombay, Maharashtra, Mumbai 400076, India
E-mail: rajaraman@chem.iitb.ac.in

Supporting information for this article is available on the WWW under https://doi.org/10.1002/chem.202402868

Among these twenty complexes, five complexes (Figure 1) [{(Me$_3$Si)$_2$ N]$_2$Gd(THF)} $_2$(μ-η^2:η^2-N$_2$)] (**1**)[18], [Gd(Hbpz$_3$)$_2$(dtbsq)] (**2**)[19], [Gd(hfac)$_3$(IM-2py)] (**3**)[20], [Gd(hfac)$_3$(NITBzImH)] (**4**)[21] and [Gd(hfac)$_3${2Py-NO}(H$_2$O)] (**5**)[22] (Figure 1) based on diversification in the structure and response to the electric field were chosen to provide a detailed insight into their magnetic characteristics under OEEF. Particularly, we aim to untangle the following intriguing questions (i) how does OEEF alter the structural parameters which are essential for controlling the *J* values? (ii) how important is the nature of co-ligand and/or rigidity of the radical moiety in controlling the magnetic exchange? (iii) Is it possible to employ OEEF to switch the sign of magnetic exchange? (iv) Is it possible to translate the study from isotropic Gd^{III} complexes to anisotropic Dy^{III} complexes to yield better SMMs?

Computational Details

Geometry optimisations were conducted using density functional theory (DFT) calculations with the Gaussian 09 package,[23] employing the hybrid B3LYP functional.[24] For Gd^{III} atoms, the CSDZ basis set[25] was chosen due to its accuracy in representing the electron distribution and interactions characteristic of these heavy elements. The 6–31 G* basis set was used for all other atoms in the study to ensure a reasonable compromise between accuracy and computational demand. The optimisation in the presence of OEEF ranging

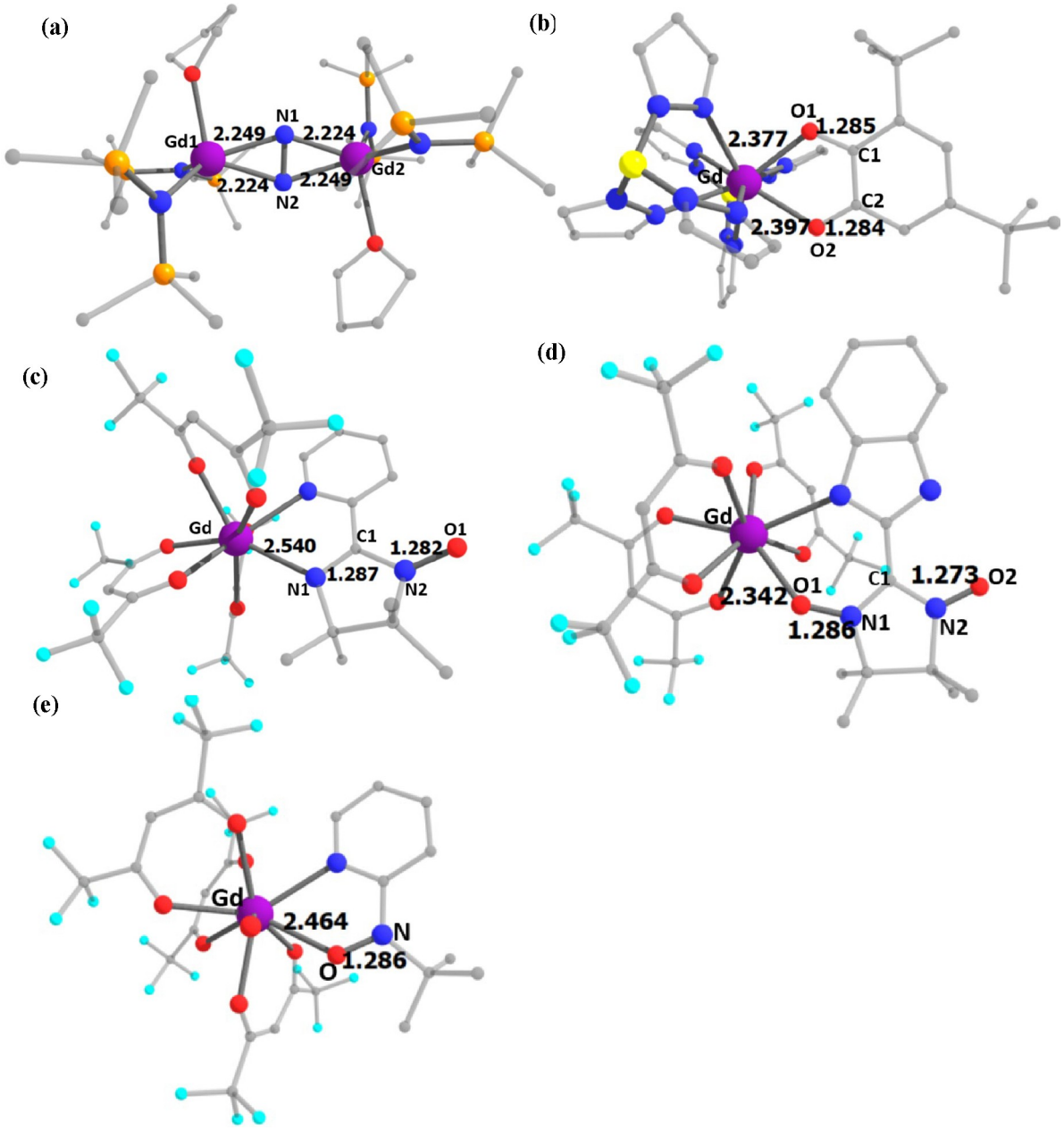

Figure 1. X-Ray structures of (a) **1** [{[(Me$_3$Si)$_2$ N]$_2$Gd(THF)}$_2$(μ-η^2: η^2-N$_2$)]$^{-\cdot}$ (b) **2** [Gd(Hbpz$_3$)$_2$(dtbsq)], (c) **3** [Gd(hfac)$_3$(IM-2py)], (d) **4** [Gd(hfac)$_3$(NITBzImH)], (e) **5** [Gd(hfac)$_3${2Py-NO}(H$_2$O)]. Colour code: purple - Gd^{III}, red - O, blue - N, cyan - F, light grey - C, orange - Si, yellow - B, green - F. Here hydrogens are omitted for clarity.

from 0.1 to 5 V/Å was implemented using the Field keyword in the Gaussian 09 software,[23] allowing for precise control over the electric field's intensity and direction. NBO (Natural Bonding Analysis) was performed in these complexes with the same level of theory and basis sets.

To determine the exchange coupling constants, Noodleman's broken symmetry[26] method was employed. This method is particularly effective for studying magnetic systems as it accurately calculates exchange interactions by comparing high-spin and broken symmetry states. The CSDZ basis set[25] was again used for Gd^{III}, while the TZV basis set was employed for the remaining atoms. Two spin states were computed for molecules **2**–**5**: one high-spin state and one broken symmetry state. In the case of molecule **1**, a more comprehensive approach was taken, with four spin states being calculated, including one high-spin state and three broken symmetry states. This thorough analysis allows for a deeper understanding of the magnetic interactions within this molecule.

$$\hat{H} = -2[J_1 S_{Gd1}.S_{rad} + J_2 S_{Gd2}.S_{rad} + J_3 S_{Gd1}.S_{Gd2}] \text{ For molecule } \mathbf{1}$$

$$\hat{H} = -2JS_{Gd}.S_{rad} \text{ For molecules } \mathbf{2}-\mathbf{5}$$

In this context, S_{Gd} and S_{rad} represent the spins associated with Gd^{III} and the radical, which are 7/2 and 1/2, respectively. The symbol J denotes the isotropic exchange coupling constant, where positive J values indicate ferromagnetic coupling and negative J values indicate antiferromagnetic coupling. The magnetic anisotropy, spin relaxation energy barriers, and g-tensors were determined from first principles using the MOLCAS 8.2 software suite.[27] For lanthanides (Ln), the ANO-RCC-VTZP basis set[28] was employed to achieve high accuracy in representing the electronic structure. For all other elements, the ANO-RCC VDZP basis set was used. The Douglas-Kroll-Hess (DKH) Hamiltonian[29] was applied to incorporate the relativistic effects that are significant in heavy metal centres such as lanthanides.

In the Complete Active Space Self-Consistent Field (CASSCF)[30] calculations, seven Ln^{III} sextets were selected as active spaces, with guess orbitals generated beforehand to facilitate the calculations. Spin-free energies were obtained via CASSCF, and these energies were further refined using Restricted Active Space State Interaction with Spin-Orbit coupling (RASSI-SO) to generate spin-orbit coupled states from 21 sextets. The g-tensors were then extracted using the SINGLE_ANISO module.[31] To manage the computational demands, disk usage was optimised through Cholesky decomposition, a technique that reduces the memory and storage requirements without sacrificing accuracy. After calculating the anisotropies of individual metal centres, the POLY_ANISO module,[32] in conjunction with the Lines model, was used to evaluate the energy of the exchange-coupled system. For the optimisations in the presence of OEEF, We have selected the positive x-axis as the axis that contains the Gd-radical part of the molecules whereas y and z axes are perpendicular to the Gd-radical part of the structure. The electric field () fields all the way from 5 V/Å to −5 V/Å were applied in various structures. Experimentally field as high as 0.37 V/Å, has been demonstrated for organic reactions and transformations,[12] it is important to note that metal complexes, which have stronger metal-ligand bonds, require a greater electric field to induce changes in the molecule. Here, we have used the notation $\mathbf{A}_{\mathbf{z+0.1}}$, which denotes the geometry of A when 0.1 V/Å OEEF is applied along the +Z-direction.

Results and Discussion

Modulation of Exchange Interactions in Complexes 1 and 2

Previous studies suggest that the net exchange interaction in these complexes comprises two contributions: J_{AF} (antiferromagnetic part) and J_F (ferromagnetic part). Generally, the J_F contribution arises due to orbital orthogonality and charge transfer to the Gd^{III} empty 5 d or 6 s orbital. Conversely, the J_{AF} contribution arises solely from the direct overlap between the 4f magnetic orbitals of Gd^{III} and the singly occupied molecular orbitals (SOMOs) of the radical ligand (Scheme S1).

In complex **1** (Figure 1(a)), both Gd^{III} centers exhibit a spin density of approximately 7.060, while two N atoms on the N_2^{3-} moiety carry spin densities of around 0.420 and 0.450 (Figure (2a)). Three types of exchange interactions were identified in this complex, namely $J_{Gd1\text{-}rad}$, $J_{Gd2\text{-}rad}$, and $J_{Gd1\text{-}Gd2}$ (refer to computational details). The initial structure displayed relatively strong antiferromagnetic exchange, with values of $J_{Gd1\text{-}rad} = -23.975\ cm^{-1}$, $J_{Gd2\text{-}rad} = -23.704\ cm^{-1}$, and $J_{Gd1\text{-}Gd2} = -0.500\ cm^{-1}$. These values closely match the experimentally reported $J_{Gd1\text{-}rad} = J_{Gd2\text{-}rad} = -27.0\ cm^{-1}$ and $J_{Gd1\text{-}Gd2} = -0.5\ cm^{-1}$. To further explore the effects of an oriented external electric field (OEEF) on these interactions, we applied electric fields ranging from +5 V/Å to −5 V/Å along the x, y, and z directions. In the presence of an oriented external electric field (OEEF) applied along the ±x, ±y, and ±z directions, the exchange interaction $J_{Gd1\text{-}rad}$ varied significantly. Along the ±x direction $J_{Gd1\text{-}rad}$ vary in the range of $-20.4\ cm^{-1}$ to $-28.1\ cm^{-1}$, along the ±y direction from $-4.7\ cm^{-1}$ to $-24.0\ cm^{-1}$, and along the ±z direction from $-18.4\ cm^{-1}$ to $-28.6\ cm^{-1}$ (Table S2). Similarly, $J_{Gd2\text{-}rad}$ varied from $-23.4\ cm^{-1}$ to $-28.5\ cm^{-1}$, from $-3.5\ cm^{-1}$ to $-22.9\ cm^{-1}$, and from $-20.6\ cm^{-1}$ to $-27.8\ cm^{-1}$ along ±x, ±y and ±z directions. (Table S2). Our detailed analysis of structural parameters that were altered under the OEEF suggests that variations in J values were correlated with the Gd1 − N1 − N2 − Gd2 torsional angle (refer to Table S3 and Figure 3(a)). Specifically, the antiferromagnetic exchange demonstrates a direct proportionality to the Gd1 − N1 − N2 − Gd2 angle (as illustrated in Figure 3(a)). This torsional angle varied from 179.0° to 178.2° along the ±x direction, from 137.9° to 151.2° along the ±y direction, and from 179.8° to 163.3° along the ±z direction (Table S3), reflecting the variation in the J observed.

We established magneto-electric-structural correlations by plotting the computed $J_{Gd\text{-}rad}$ coupling constant against the Gd1 − N1 − N2 − Gd2 dihedral angles under various OEEF conditions (Figure 3(a)). Larger dihedral angles, yielding a planar $\{Gd_2N_2\}$ motif, showed stronger antiferromagnetic (AF) exchange, primarily driven by the π* SOMOs of N_2^{3-} overlapping with the $4f_{y(3x^2-y^2)}$ orbitals of the Gd^{III} ions. The $\{Gd_2N_2\}$ moiety exhibited maximum bending at an OEEF of $\mathbf{1}_{y+4.3}$ V/Å, with a dihedral angle of 137.9° ($J_{Gd1\text{-}rad} = -4.7\ cm^{-1}$), ($J_{Gd2\text{-}rad} = -3.5\ cm^{-1}$), and ($J_{Gd\text{-}Gd} = -0.2\ cm^{-1}$) (Table S2). Although further bending at higher OEEF levels was expected to render $J_{Gd\text{-}rad}$ ferromagnetic, steric clashes between $NSiMe_3$ groups impeded this possibility. Therefore, in complex **1**, OEEF can only

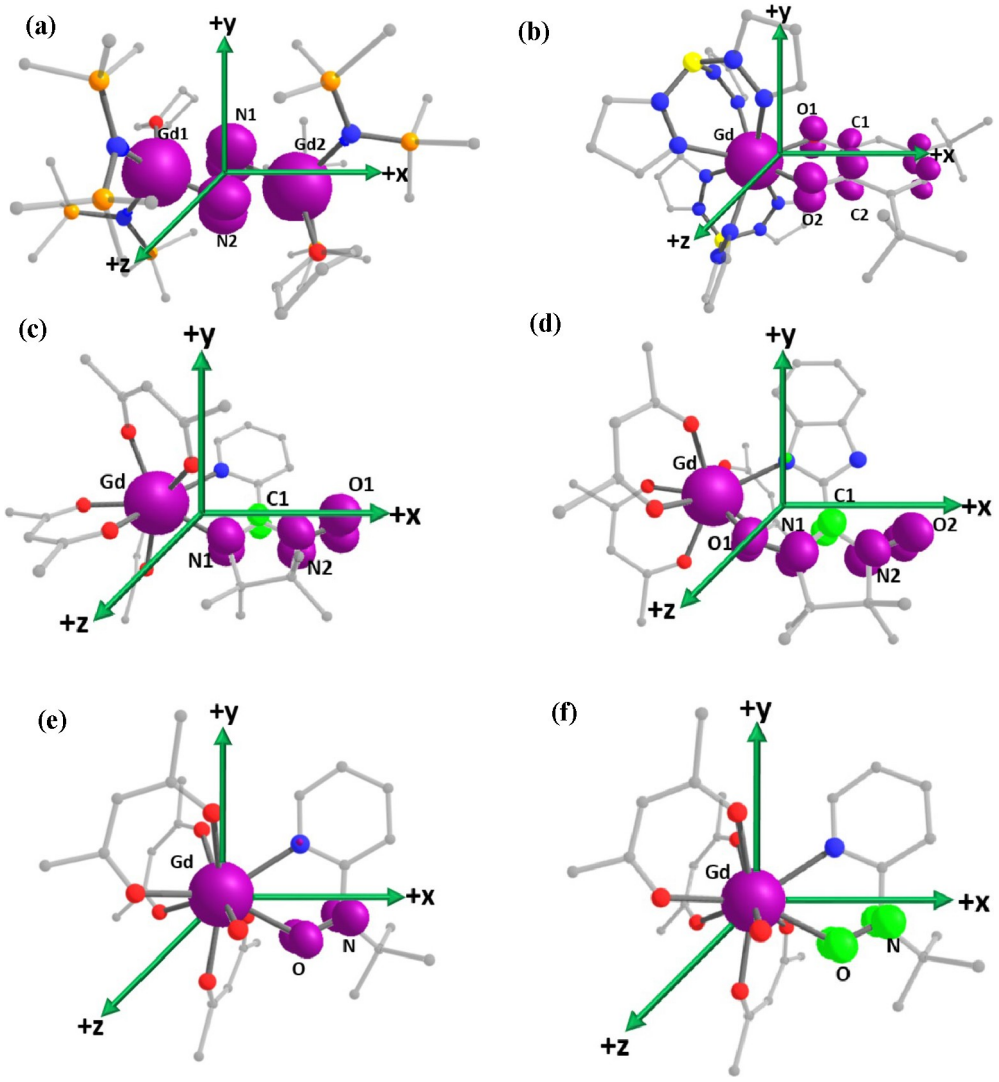

Figure 2. Spin density plots of (a) **1** $[\{[(Me_3Si)_2N]_2Gd(THF)\}_2(\mu\text{-}\eta^2\text{:}\eta^2\text{-}N_2)]^-$, (b) **2** $[Gd(Hbpz_3)_2(dtbsq)]$, (c) **3** $[Gd(hfac)_3(IM\text{-}2py)]$, (d) **4** $[Gd(hfac)_3(NITBzImH)]$, (e) **5** $[Gd(hfac)_3\{2Py\text{-}NO\}(H_2O)]$ and (f) optimized structure of $\mathbf{5}_{y+2.5}$ with computed spin density for broken symmetry. Colour code: purple - Gd^{III}, red - O, blue - N, cyan - F, light grey - C, orange - Si, yellow - B, green - F. Magneta and green colored surface shows the spin density present with isosurface 0.006 e^- $bohr^{-3}$. Here hydrogens and fluorine are omitted for clarity.

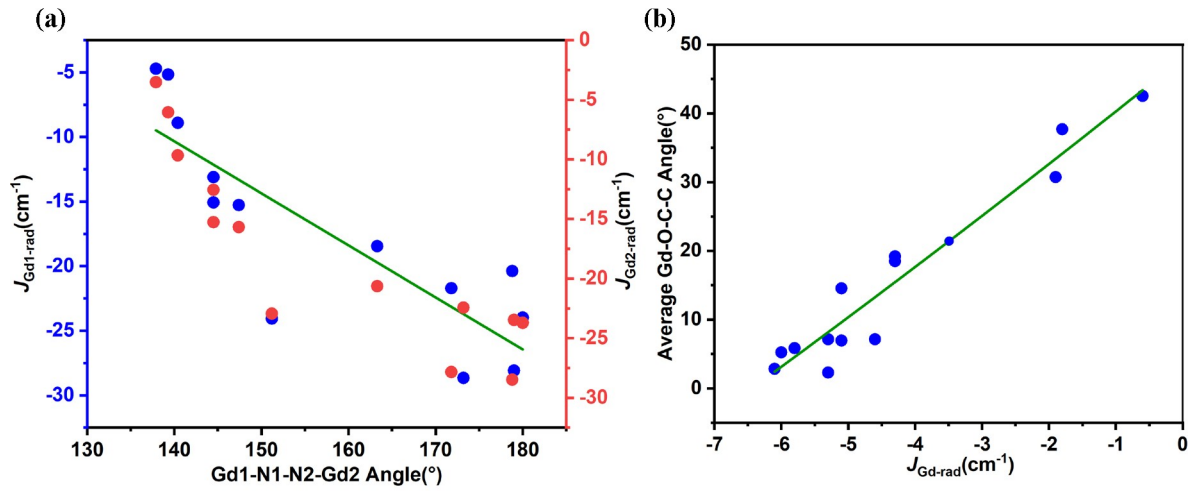

Figure 3. (a) Plot of Gd1 – N1 – N2 – Gd2 torsional angles observed for various geometries under OEEFs and $J_{Gd1\text{-}rad}$ and $J_{Gd2\text{-}rad}$ in **1**, (b) Plot of $J_{Gd1\text{-}rad}$ versus Gd – O1(O2) – C1(C2) – C2(C1) torsional angles computed under various OEEFs in **2**.

moderately decrease AF exchange, and substantial sign reversal and enhancement are hindered by complex geometric arrangements, leading to undesired structural alterations. Given these limitations, we shifted our focus to another type of Gd-radical complex and chose a semiquinone radical moiety as our next target (complex **2**). This adjustment was aimed at overcoming the geometric constraints and exploring the potential for achieving a switch in *J* with respect to OEEF.

In **2** (Figure 1(b)), the Gd center exhibits a spin density of 7.046, while two oxygen atoms of the quinone ligands carry spin densities of 0.240 each (Figure 2(b)). Additionally, a spin density of 0.507 is delocalized across the benzene ring adjacent to the two oxygen atoms of the quinone(Figure 2(b)). In complex **2** (Figure 1(b)), where $J_{Gd\text{-}rad}$ is calculated as $-6.0\ cm^{-1}$, experimentally determined as $-5.7\ cm^{-1}$, and optimised to $-5.8\ cm^{-1}$, the exchange interaction was studied under the influence of an oriented external electric field (OEEF) along the $\pm x$, $\pm y$, and $\pm z$ directions. Along the $\pm x$ direction, $J_{Gd\text{-}rad}$ varied from $-4.6\ cm^{-1}$ to $-6.1\ cm^{-1}$. In the $\pm y$ direction, it ranged from $-0.6\ cm^{-1}$ to $-4.3\ cm^{-1}$; in the $\pm z$ direction, it ranged from $-4.3\ cm^{-1}$ to $-5.8\ cm^{-1}$ (Table S4). The smallest antiferromagnetic exchange was observed for the configuration $\mathbf{2}_{y+3}$, with $J_{Gd\text{-}rad}$ being $-0.6\ cm^{-1}$. The variation in *J* values with the direction of the electric field was linked to changes in the Gd−O−C−C dihedral angle, which increased with the $+x$ direction and decreased with the $-x$ direction, following a linear relationship (Table S4-S5 and Figure 3(b)). The maximum dihedral angle reached was 42.5°, constrained by steric factors.

Additionally, the semiquinonate radical in complex **2** has a significantly delocalised spin density, resulting in only minor variations in the exchange interactions. This suggests that radicals with more localised spin densities would be better suited for modulating the exchange interactions effectively. Therefore, to achieve a more significant modulation of the *J* values, we propose investigating complex **3**, which contains radicals with more localised spin densities. By exploring the effects of OEEF on these complexes, we aim to understand better the interplay between structural parameters and magnetic exchange interactions, ultimately guiding the design of materials with tunable magnetic properties.

Modulation of Exchange Interactions in Complexes 3 and 4:

In complex **3** (Figure 1(c)), the Gd^{III} center exhibits a spin density of 7.030, while the ring's N1 carries a spin density of 0.347, the N2(NO) bears 0.247, and the O(NO) possesses 0.467 (Figure 2(c)). Complex **3** exhibits a J_{Gd-rad} value of $-2.3\ cm^{-1}$, with experimentally determined $J_{exp} = -3\ cm^{-1}$ and optimised $J_{opt} = -1.9\ cm^{-1}$. In the presence of OEEF, the J_{Gd-rad} values varied along the $\pm x$ direction from $-1.8\ cm^{-1}$ to $-2.0\ cm^{-1}$, along the $\pm y$ direction from $-1.9\ cm^{-1}$ to $-2.1\ cm^{-1}$, and the $\pm z$ direction from $-1.8\ cm^{-1}$ to $-2.0\ cm^{-1}$ (Table S6).

Applying the electric field in the $\pm x$, $\pm y$, and $\pm z$ directions did not significantly alter the angles or dihedrals within complex **3**. However, variations were observed in the Gd–N1 bond distance, which ranged from 2.4 Å to 2.6 Å (Table S7 and Figure 4(a))). As the Gd–N1 bond distance increased, the J_{Gd-rad} decreased, consistent with the expected drop in π^* SOMO-4f overlap (Figure 4(a) and Table S7). Although a switch in the *J* value was not observed, the magnitude of the antiferromagnetic interactions reached a minimum at the $\mathbf{3}_{z+3}$ point, where the Gd–N1 bond distance was significantly elongated to 2.6 Å (Table S7). The inability to switch the *J* value is attributed to the minimal influence of angle and dihedral alterations on the *J* values, as the atom with the dominant radical character is not directly connected to the Gd^{III} centres.

This observation suggests that to modulate the *J* values effectively, it is crucial to select molecules where the radical character is directly associated with the Gd^{III} centres. This insight provides a guiding principle for designing and choosing the appropriate set of molecules to achieve significant changes in exchange interactions under the influence of an electric field.

In complex **4** (Figure 1(d)), the Gd^{III} center exhibits a spin density of 7.031, while the ring's O1 carries a spin density of 0.319, N1 on the ring has 0.274, N2(NO) has 0.311, and O2(NO)

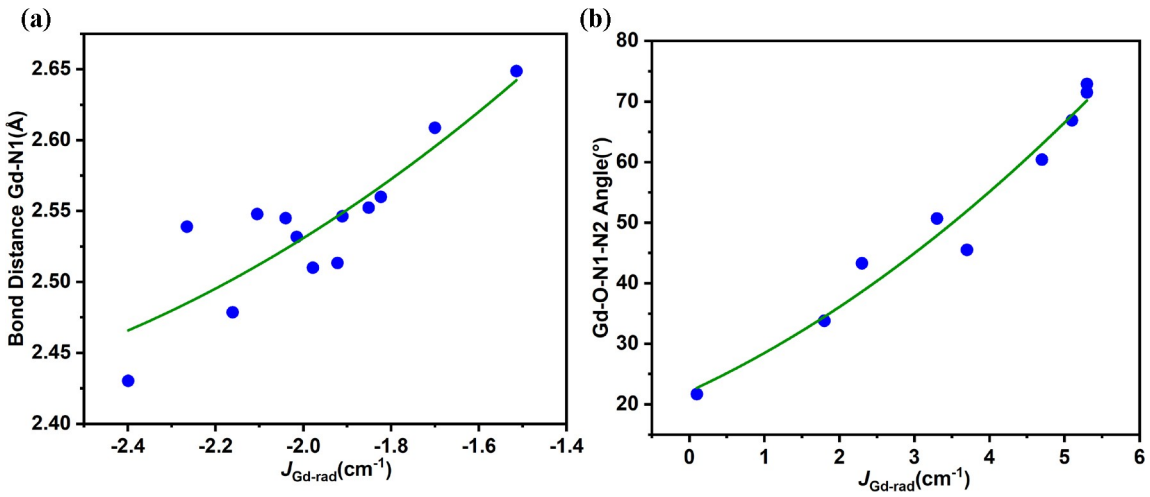

Figure 4. (a) Plot between Gd–N1(lig) and *J* in **3**, (b) Plot between and $J_{Gd1\text{-}rad}$ and Gd−O−N1(NO1)−N2(NO2) torsional angles in **4**.

bears 0.291 (Figure 2(d)). Complex **4** (Figure 1(d)) features a nitronyl nitroxide radical exhibiting a ferromagnetic J_{Gd-rad} interaction. It has a J_{Gd-rad} exchange of $+1.9\ cm^{-1}$, while the experimentally reported value is $+1.7\ cm^{-1}$. When subjected to an oriented external electric field (OEEF), the J_{Gd-rad} was found to vary along the $\pm x$ direction from $+3.7\ cm^{-1}$ to $+4.7\ cm^{-1}$, along the $\pm y$ direction from $+3.3\ cm^{-1}$ to $+5.1\ cm^{-1}$, and the $\pm z$ direction from $+0.1\ cm^{-1}$ to $+5.3\ cm^{-1}$ (see Table S8).

The OEEF predominantly altered the Gd–O–N1(NO1)–N2(NO2) dihedral angle (Figure 4(b) and Table S9). As this angle increased, the J_{Gd-rad} tended to become more ferromagnetic. This effect is attributed to a larger charge transfer from the singly occupied molecular orbital (SOMO) to the 5 d orbital of the Gd^{III} ion and a reduction in the π^*-4f overlap. At the $\mathbf{4}_{z+3.4}$ configuration, the ferromagnetic *J* reached a maximum value of $+5.3\ cm^{-1}$, limited by the largest dihedral angle attainable before steric strain was triggered.

These observations demonstrate that ferromagnetic coupling can be enhanced by applying an electric field in this class of molecules. Encouraged by these results, we chose another class of nitronyl nitroxide radical, which exhibits antiferromagnetic coupling, to see if the sign of J can be altered (complex **5**).

Modulation of Exchange Interactions in Complex 5

Next, our focus shifted to complex **5** (depicted in Figure 1(e)), where the $NO^{\bullet}$ radical is directly bound to the Gd^{III} center. In this configuration, the spin density on the Gd^{III} was determined to be 7.035, while the N and O atoms exhibit spin densities of 0.429 and 0.437, respectively (Figure 2(e)), indicating the localized nature of the radical. In complex **5** (Figure 1 (e)), where the nitronyl nitroxide radical ($NO^{\bullet}$) is directly bound to the Gd^{III} centre, the J_{Gd-rad} exchange is calculated as $-3.7\ cm^{-1}$, with the experimentally reported value being $-4.8\ cm^{-1}$. Under the influence of an oriented external electric field (OEEF), the J_{Gd-rad} values varied along the $\pm x$ direction from $+1.8\ cm^{-1}$ to $+3.3\ cm^{-1}$, along the $\pm y$ direction from $-1.9\ cm^{-1}$ to $+5.5\ cm^{-1}$, and the $\pm z$ direction from $-3.8\ cm^{-1}$ to $+4.1\ cm^{-1}$ (Table S10 and Figure 5(a)). Notably, the application of the electric field could switch the J_{Gd-rad} exchange from antiferromagnetic to ferromagnetic, except in the $-y$ and $-z$ directions within the field strength range of 1 to 3 V/Å. The highest ferromagnetic exchange was estimated to be $+5.5\ cm^{-1}$ in the configuration $\mathbf{5}_{y+2.5}$ (Table S10).

Several structural parameters varied under the applied electric field, with significant geometric changes observed in

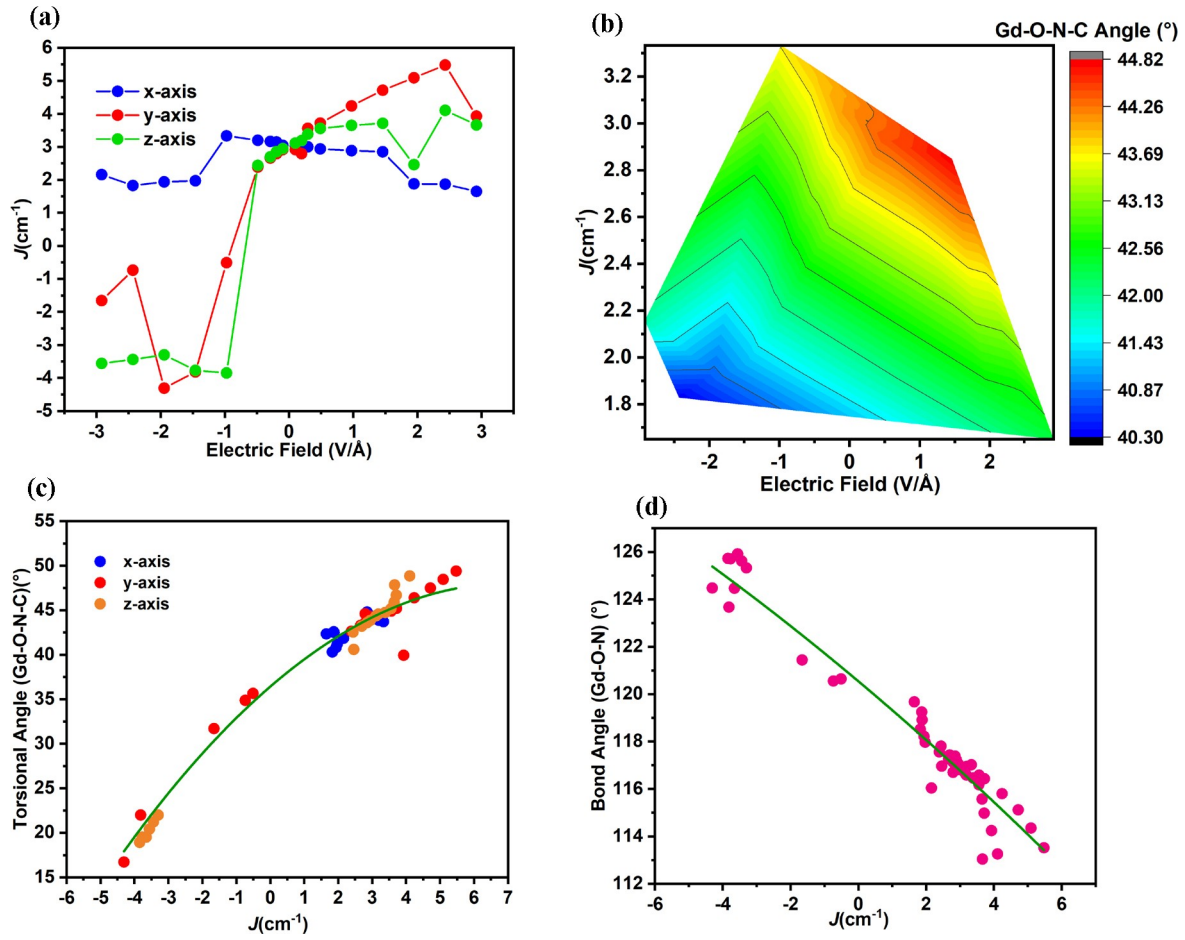

Figure 5. (a) plot between J_{Gd-rad} and OEEF applied in **5**, (b) 3D Plot between Gd–O–N–C torsional angle and the OEEF applied in different geometries of **5** and J_{Gd-rad}, (c) plot between the Gd–O–N–C torsional angle and the J_{Gd-rad} in **5**, (d) Plot between angle Gd–O–N and the exchange coupling constants on different geometries of **5**

the Gd – O – N – C torsional angle. Plotting the torsional angles obtained for various electric field geometries against the computed J_{Gd-rad} revealed a correlation where larger angles resulted in stronger ferromagnetic J_{Gd-rad} coupling (see magneto-electrical-structural map in Figures 5(b)–5(c) and Table S11). The second most influential structural parameter was the Gd – O – N angle, where larger angles resulted in stronger antiferromagnetic exchange (Figures 5(d)). At the same time, no direct correlation was observed between exchange and the Gd–O bond distances (Figure S1). It was observed that a torsional angle greater than 35.9° resulted in ferromagnetic exchange, whereas a value less than 35.9° led to antiferromagnetic exchange (Figure 5(c)). To deeply understand the nature of the exchange in the absence and presence of OEEF, we conducted overlap integral, molecular orbital (MO), and Natural Bond Orbital (NBO) analysis on complex **5** and the configuration $\mathbf{5}_{y+2.5}$ (which exhibited the highest J_{Gd-rad} of 5.5 cm^{-1}). Based on these analyses, we proposed a generic mechanism considering all the points above, as outlined in Scheme S1 (See ESI).

The NBO analysis revealed the electronic configuration of Gd^{III} as 6 s(0.18)4 f(7.01)5d(0.76)6p(0.41) in complex **5** and 6 s(0.18)4 f(7.01)5d(0.74)6p(0.40) in configuration $\mathbf{5}_{y+2.5}$, indicating significant electron occupancy in the 6 s, 5d, and 6p orbitals due to charge transfer. Additionally, there was evidence of charge transfer from the π* SOMO of the 2Py-NO to the Gd^{III} 5d orbitals in both complex **5** (2.1 kJ/mol) and configuration $\mathbf{5}_{y+2.5}$ (1.9 kJ/mol) (Figure 6). Thus, there was no discernible difference between these two configurations regarding the ferromagnetic exchange contribution J_F.

Subsequently, we computed the overlap integral calculations to assess the overlap between the 2Py-NO SOMO π* orbitals and the Gd^{III} 4 f orbitals. In complex **5**, three significant overlap integrals were observed (Figure S2 and Table S12), whereas in configuration $\mathbf{5}_{y+2.5}$, the number of significant overlap integrals was reduced to two (Figure S3 and Table S13). This reduction translated to a decreased contribution from the antiferromagnetic exchange J_{AF}, thereby shifting the overall exchange towards ferromagnetic upon applying OEEF, as desired.

As the OEEF switches from negative to a positive direction, the sign of *J* is altered and this along with the studies on complexes **1**–**5** offers the following guiding principles:

1. Radicals with SOMOs directly attached to the Gd^{III} centre provide a broad range of structural variations that influence the sign of the exchange coupling.
2. Radicals with spin densities localised on one or two centres are preferred, as they offer greater control over *J* with respect to the applied electric field and also offer a greater chance to modulate the values.
3. In a relatively rigid ligand such as hfac, structural alterations under EF are directed towards the more flexible radical moiety, facilitating extensive variations and therefore the choice of the co-ligand at the complex is also key in modulating the *J* values.
4. A co-ligand with reduced steric bulk at the Gd^{III} centres can enable larger variations in bond angles and dihedral angles, aiding in switching *J* values.

Having managed to demonstrate variation in the sign of *J* value from antiferromagnetic to ferromagnetic in complex **5**, we decided to extend the study to the Dy^{III} analogue to assess whether the quantum tunnelling of magnetisation (QTM) effects and single-ion anisotropy are enhanced under the applied EF, potentially resulting in better-performing SMMs. Consequently, SA-CASSCF/RASSI/SINGLE_ANISO calculations were performed on the corresponding Dy^{III} complex **5**-Dy ($[Dy(hfac)_3\{2Py\text{-}NO\}(H_2O)]$). In **5**-Dy the g-tensors are found as g_{xx} = 0.170, g_{yy} = 0.246 and g_{zz} = 19.720, and the angle between the ground state and the first excited state is 12.9° (Table S14). Further, we have performed the Poly_Aniso calculations in order to account for the exchange coupled system and to derive the relaxation mechanism for the Dy(III)-radical system. Our analysis revealed that complex **5**-Dy exhibited remarkably high tunnel splitting, making it unsuitable for SMM properties. However, in nearly all the geometries under applied OEEF conditions, the tunnel splitting decreased signifi-

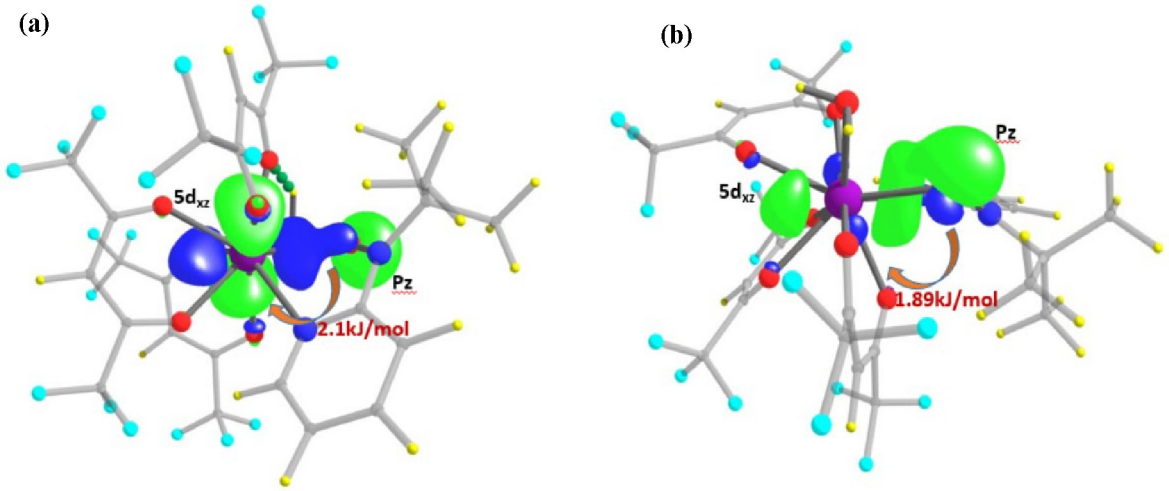

Figure 6. NBO analysis showing charge transfer from (a) π* orbitals of Py-NO to $5d_{xz}$ orbitals of Gd^{III} orbitals in **5**, (b) π* orbitals of Py-NO to $5d_{xz}$ orbitals of Gd^{III} orbitals in $\mathbf{5}_{y+2.5}$. Colour code: purple - Gd^{III}, red - O, blue - N, cyan - F, light grey - C, orange - Si, yellow - B, green - F.

cantly, enabling relaxation from the first excited state (refer to Table S15) and improving the SMM performance. We observed that the **5**-$Dy_{y+2.5}$ was showing the highest energy barrier for the spin-reversal. The first excited state in complex **5**-Dy was found to be at 46.3 cm^{-1}, whereas, for **5**-$Dy_{y+2.5}$, it was at 59.1 cm^{-1} (Single ion property) (refer to Table S14), suggesting that there is marginal improvement in single-ion anisotropy at this chosen field strength. Furthermore, the ground state g_{zz} axis of **5**-$Dy_{y+2.5}$ is slightly tilted towards the 2Py-NO radical ligand compared to **5** (Figure 7(b)).

Furthermore, we found a correlation between the energy barrier for demagnetization and the exchange coupling strength. The highest energy barrier of 24.7 cm^{-1} (Figure 7(a)) was observed for **5**-$Dy_{y+2.5}$, which also exhibited the strongest exchange coupling. This is consistent with the enhanced single-molecule magnet (SMM) behaviour observed upon applying an electric field.

Conclusions

In conclusion, our investigation underscores the capability of OEEF to manipulate magnetic properties within 4f-radical systems intricately. This capability opens avenues for customising functionalities, notably by enabling the transformation of magnetic exchange from antiferromagnetic to ferromagnetic states. Our study offers significant insights into the strategic selection of molecules that exhibit optimal responses to applied electric fields (EF). Specifically, we observed enhanced performance in the context of anisotropic Dy^{III} analogues under EF conditions. The following summary emerges from this work:

1. **Magneto-Electric-Structural Correlations**: The application of OEEF in various directions significantly affects the exchange interactions in metal complexes, particularly in terms of magnetic behaviour and structural changes, such as the torsional angles between metal and ligand atoms. There is a correlation between dihedral angles and magnetic exchange interactions, where larger angles tend to enhance antiferromagnetic exchange due to improved orbital overlap between the ligands and metal ions.
2. **Sensitivity of Exchange Interactions**: The exchange interactions are sensitive to the direction and magnitude of the applied electric field, with notable variations observed in different complexes, indicating the potential for fine-tuning magnetic properties through external electric fields. Among various complexes studied, in complex **4**, the application of OEEF significantly enhanced $J_{Gd\text{-}rad}$ ferromagnetic coupling along the +x, +y and +z directions. The dihedral angle changes under the electric field led to increased charge transfer and reduced π*-4f overlap, resulting in stronger ferromagnetic interactions.
3. **Role of Radical Character**: The nature of the radical's spin density is crucial in modulating exchange interactions. Radicals with localized spin densities are far more effective at achieving significant changes in these interactions compared to those with delocalized spin densities. This is because localized spin densities provide a more direct and substantial influence on the magnetic properties of the complex. Moreover, complexes in which the radical is directly linked to the metal centre are particularly advantageous for fine-tuning via OEEF. Direct linkage ensures a more pronounced impact of the electric field on the exchange interactions, enabling precise and efficient modulation.
4. **Potential for Ferromagnetic Coupling**: In certain complexes, the application of OEEF can switch the exchange interaction from antiferromagnetic to ferromagnetic. This highlights the importance of structural adjustments and charge transfer mechanisms in enhancing magnetic coupling, which can be leveraged to design materials with tunable magnetic properties. For instance, in complex **5**, we observed this switch from antiferromagnetic to ferromagnetic interaction even at low electric field strengths, demonstrating the potential for efficient magnetic modulation under mild conditions. Evidence of charge transfer from the π* SOMO of 2Py-NO to the

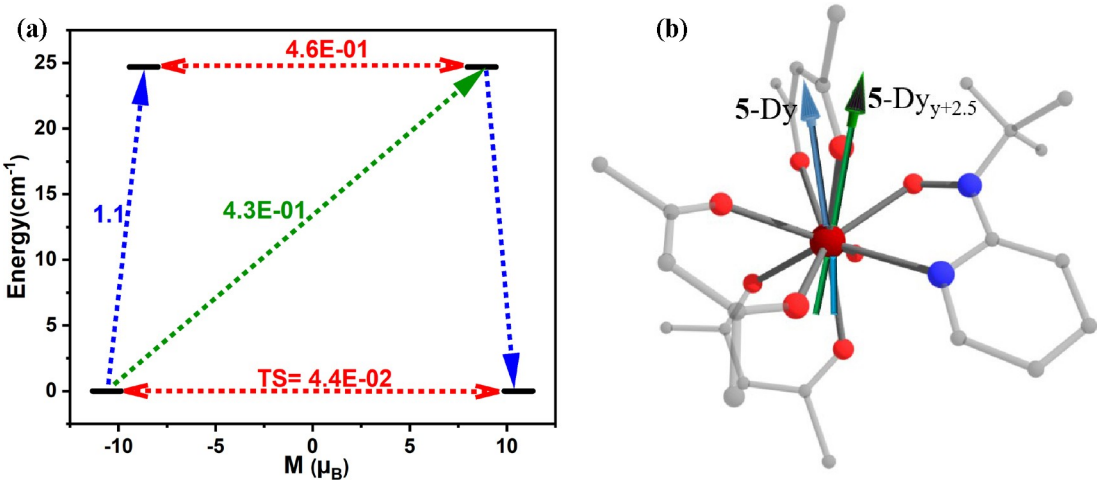

Figure 7. (a) ground state g_{zz} axis in **5**-Dy and **5**-Dy_{y+2}, and (b) Magnetic relaxation mechanism (exchange coupled) of **5**-$Dy_{y+2.5}$ (Here, red dotted lines indicate tunnel splitting (TS), and the green dotted lines indicate Orbach/Raman relaxation). Here hydrogen and fluorine are omitted for clarity. Colour code: maroon - Dy^{III}, red - O, blue - N, cyan - F, light grey - C, orange - Si, yellow - B, green - F. Here hydrogens and fluorine are omitted for clarity.

Gd^{III} 5 d orbitals was found in both complex **5** and configuration $\mathbf{5}_{y+2.5}$, showing no discernible difference in ferromagnetic exchange contribution. The switch was observed at all fields along the x-axis, whereas in the y and z directions, it was present at all electric fields except for those ranging from −1 to −3 V/Å.

5. **Elevation of the Demagnetization Energy Barrier through OEEF**: We have observed that there is a correlation between the exchange coupling and the energy barrier for the spin reversal. $\mathbf{5}$-$Dy_{y+2.5}$ was found to have the highest exchange coupling of $+5.5\ cm^{-1}$ and, consequently, has the highest energy barrier of $24.5\ cm^{-1}$ as well.

By harnessing OEEF, we expand the understanding of how magnetic interactions can be controlled at the molecular level and pave the way for potential applications in advanced materials and molecular electronics. This work highlights the profound impact of external stimuli on molecular magnetism, laying a foundation for future research to develop tailored magnetic properties for various technological applications.

Acknowledgements

TS is thankful to IRCC for fellowship. GR would like to thank SERB (SB/SJF/2019-20/12; CRG/2022/001697) for funding.

Conflict of Interests

The authors declare no conflict of interest.

Data Availability Statement

The data that support the findings of this study are available in the supplementary material of this article.

Keywords: Oriented External Electric Field · exchange coupling · Lanthanide-radical complexes · magnetic anisotropy · single molecule magnet · molecular nano magnets

[1] a) R. Sessoli, A. K. Powell, *Coordination Chemistry Reviews* **2009**, *253*, 2328–2341; b) V. Vieru, S. Gómez-Coca, E. Ruiz, L. F. Chibotaru, *Angewandte Chemie* **2024**, *136*, e202303146; c) A. Swain, T. Sharma, G. Rajaraman, *Chemical Communications* **2023**, *59*, 3206–3228.
[2] M. K. Singh, N. Yadav, G. Rajaraman, *Chemical communications* **2015**, *51*, 17732–17735.
[3] S. V. Eliseeva, M. Ryazanov, F. Gumy, S. I. Troyanov, L. S. Lepnev, J. C. G. Bünzli and N. P. Kuzmina in *Dimeric Complexes of Lanthanide (III) Hexafluoroacetylacetonates with4-Cyanopyridine N-Oxide: Synthesis, Crystal Structure, Magnetic and Photoluminescent Properties*, Vol. Wiley Online Library, **2006**.
[4] N. Ahmed, T. Sharma, L. Spillecke, C. Koo, K. U. Ansari, S. Tripathi, A. Caneschi, R. D. Klingeler, G. Rajaraman, M. Shanmugam, *Inorganic Chemistry* **2022**, *61*, 5572–5587.
[5] S. F. Schmidt, M. P. Merkel, G. E. Kostakis, G. Buth, C. E. Anson, A. K. Powell, *Dalton Transactions* **2017**, *46*, 15661–15665.
[6] H.-S. Wang, K. Zhang, Y. Song, Z.-Q. Pan, *Inorganica Chimica Acta* **2021**, *521*, 120318.
[7] Y.-Z. Ma, L.-M. Zhang, G. Peng, C.-J. Zhao, R.-T. Dong, C.-F. Yang, H. Deng, *CrystEngComm* **2014**, *16*, 667–683.
[8] R. Maurice, T. Mallah and N. Guihéry in *Magnetism in Binuclear Compounds: Theoretical Insights*, Springer **2023**, pp. 207–233.
[9] T. Rajeshkumar, G. Rajaraman, *Chemical Communications* **2012**, *48*, 7856–7858.
[10] A. Bleuzen, V. Marvaud, C. Mathoniere, B. Sieklucka, M. Verdaguer, *Inorganic chemistry* **2009**, *48*, 3453–3466.
[11] a) S. Hoffmann, J. Goslar, W. Hilczer, M. Krupski, *Inorganic Chemistry* **1993**, *32*, 3554–3556; b) Y. Cui, Y. Wu, Y. Li, R. Liu, X. Dong, Y. Wang, *Science China Physics, Mechanics & Astronomy* **2014**, *57*, 1299–1303.
[12] a) S. A. C. Aragones, N. L. Haworth, N. Darwish, S. Ciampi, N. J. Bloomfield, G. G. Wallace, I. Diez-Perez, M. L. Coote, *Nature* **2016**, *531*, 88–91; b) A. Sarkar, G. Rajaraman, *Chemical Science* **2020**, *11*, 10324–10330; c) R. K. Tiwari, R. Paul and G. Rajaraman, *Dalton Transactions* **2024**, *53*, 14623–14633
[13] M. Fittipaldi, A. Cini, G. Annino, A. Vindigni, A. Caneschi, R. Sessoli, *Nature materials* **2019**, *18*, 329–334.
[14] a) G. M. Gutiérrez-Finol, S. Giménez-Santamarina, Z. Hu, L. E. Rosaleny, S. Cardona-Serra, A. Gaita-Ariño, *npj Computational Materials* **2023**, *9*, 196; b) G. Aromí and O. Roubeau in *Lanthanide molecules for spin-based quantum technologies*, *Vol. 56* Elsevier, **2019**, pp. 1–54; c) G. Aromí, F. Luis and O. Roubeau, *Lanthanides and actinides in molecular magnetism* **2015**, 185–222; d) R. Sessoli in *Toward the quantum computer: magnetic molecules back in the race*, Vol. ACS Publications, **2015**.
[15] A. Palii, B. Tsukerblat, S. Klokishner, S. Aldoshin, D. Korchagin, J. M. Clemente-Juan, *The Journal of Physical Chemistry C* **2018**, *123*, 2451–2459.
[16] a) C. A. Goodwin, F. Ortu, D. Reta, N. F. Chilton, D. P. Mills, *Nature* **2017**, *548*, 439–442; b) F.-S. Guo, B. M. Day, Y.-C. Chen, M.-L. Tong, A. Mansikkamäki, R. A. Layfield, *Science* **2018**, *362*, 1400–1403; c) C. A. Gould, K. R. McClain, D. Reta, J. G. Kragskow, D. A. Marchiori, E. Lachman, E.-S. Choi, J. G. Analytis, R. D. Britt, N. F. Chilton, *Science* **2022**, *375*, 198–202.
[17] a) C. Lescop, E. Belorizky, D. Luneau, P. Rey, *Inorganic chemistry* **2002**, *41*, 3375–3384; b) H. Zhao, J. Bazile, J Mervin, J. R. Galán-Mascarós, K. R. Dunbar, *Angewandte Chemie International Edition* **2003**, *42*, 1015–1018.
[18] J. D. Rinehart, M. Fang, W. J. Evans, J. R. Long, *Nature Chemistry* **2011**, *3*, 538–542.
[19] A. Caneschi, A. Dei, D. Gatteschi, L. Sorace, K. Vostrikova, *Angewandte Chemie International Edition* **2000**, *39*, 246–248.
[20] T. Tsukuda, T. Suzuki, S. Kaizaki, *Journal of the Chemical Society, Dalton Transactions* **2002**, 1721–1726.
[21] C. Lescop, D. Luneau, P. Rey, G. Bussière, C. Reber, *Inorganic chemistry* **2002**, *41*, 5566–5574.
[22] T. Ishida, R. Murakami, T. Kanetomo, H. Nojiri, *Polyhedron* **2013**, *66*, 183–187.
[23] M. Frisch, *Inc, Wallingford CT* **2009**, *201*.
[24] a) A. D. Becke, *Physical review A* **1988**, *38*, 3098; b) C. Lee, W. Yang, R. G. Parr, *Physical review B* **1988**, *37*, 785; c) A. D. Becke, *The Journal of chemical physics* **1992**, *96*, 2155–2160.
[25] T. R. Cundari, W. J. Stevens, *The Journal of chemical physics* **1993**, *98*, 5555–5565.
[26] M. Dolg, U. Wedig, H. Stoll, H. Preuss, *The Journal of chemical physics* **1987**, *86*, 866–872.
[27] F. Aquilante, J. Autschbach, R. K. Carlson, L. F. Chibotaru, M. G. Delcey, L. De Vico, I. Fdez. Galván, N. Ferré, L. M. Frutos and L. Gagliardi in *Molcas 8: New capabilities for multiconfigurational quantum chemical calculations across the periodic table*, Vol. Wiley Online Library, **2016**.
[28] B. R. O. Roos, R. Lindh, P.-Å. Malmqvist, V. Veryazov, P.-O. Widmark, A. C. Borin, *Journal of Physical Chemistry A112*, pp. 11431–11435**2008**.
[29] T. Nakajima, K. Hirao, *Chemical reviews* **2012**, *112*, 385–402.
[30] L. Ungur, L. F. Chibotaru, *Chemistry–A European Journal* **2017**, *23*, 3708–3718.
[31] L. F. Chibotaru, L. Ungur, *The Journal of chemical physics* **2012**, *137*.
[32] a) L. Chibotaru, L. Ungur, A. Soncini, *Angewandte Chemie-International Edition* **2008**, *47*, 4126–4129; b) L. Ungur, W. Van den Heuvel, L. F. Chibotaru, *New Journal of Chemistry* **2009**, *33*, 1224–1230; c) L. F. Chibotaru, L. Ungur, C. Aronica, H. Elmoll, G. Pilet, D. Luneau, *Journal of the American Chemical Society* **2008**, *130*, 12445–12455.

Manuscript received: July 30, 2024
Accepted manuscript online: October 23, 2024
Version of record online: November 16, 2024